Formation of double-shelled zinc-cobalt sulfide dodecahedral cages from bimetallic zeolitic imidazolate frameworks for hybrid supercapacitors

Zhang, Peng; Guan, Bu Yuan; Yu, Le; Lou, David Xiong Wen

2017

Zhang, P., Guan, B. Y., Yu, L., & Lou, D. X. W. (2017). Formation of double-shelled zinc-cobalt sulfide dodecahedral cages from bimetallic zeolitic imidazolate frameworks for hybrid supercapacitors. Angewandte Chemie International Edition, 56(25), 7141-7145. doi:10.1002/anie.201702649

https://hdl.handle.net/10356/138608

https://doi.org/10.1002/anie.201702649

Formation of Double-Shelled Zinc-Cobalt Sulfide Dodecahedral Cages from Bimetallic Zeolitic Imidazolate Frameworks for Hybrid Supercapacitors

*Peng Zhang, Bu Yuan Guan, Le Yu and Xiong Wen (David) Lou**

[*] Dr. P. Zhang, Dr. B. Y. Guan, Dr. L. Yu, Prof. X. W. Lou

School of Chemical and Biomedical Engineering, Nanyang Technological University, 62 Nanyang Drive, Singapore, 637459, (Singapore)

Email: xwlou@ntu.edu.sg; Webpage: http://www.ntu.edu.sg/home/xwlou/

Abstract

Complex metal-organic frameworks used as precursors allow design and construction of various nanostructured functional materials which might not be possible by other methods. Here, we develop a sequential chemical etching and sulfurization strategy to prepare well-defined double-shelled zinc-cobalt sulfide (Zn-Co-S) rhombic dodecahedral cages (RDCs). Yolk-shelled zinc/cobalt-based zeolitic imidazolate framework (Zn/Co-ZIF) RDCs are first synthesized by a controlled chemical etching process, followed by a hydrothermal sulfurization reaction to prepare double-shelled Zn-Co-S RDCs. Moreover, the strategy reported in this work enables easy control of the Zn/Co molar ratio in the obtained double-shelled Zn-Co-S RDCs. Owing to the structural and compositional benefits, the obtained double-shelled Zn-Co-S RDCs exhibit enhanced performance with high specific capacitance (1266 F g^{-1} at 1 A g^{-1}), good rate capability and long-term cycling stability (91% retention over 10,000 cycles) as a battery-type electrode material for hybrid supercapacitors.

Keywords: zeolitic imidazolate frameworks; double-shelled structures; zinc-cobalt sulfide; hybrid supercapacitors.

Renewable energy technologies are of great importance in addressing the energy crisis and global environmental change.[1–4] Among various electrochemical energy storage and conversion systems, hybrid supercapacitors (HSCs) have been widely investigated in recent years because of multiple advantages of high power density, fast charge-discharge rate and excellent cycling stability.[5–7] The battery-type electrode in the HSC is the key component to build an efficient device.[8] As a result, continuous efforts have been dedicated to developing high performance battery-type electrode materials for HSCs. Among the potential electrode materials, transition metal sulfides (TMSs) are regarded as promising materials in view of their high capacitance, rich redox sites and improved conductivity compared with their corresponding metal oxides.[9] Superior to monometal sulfides, mixed metal sulfides by introduction of hetero-metal ions offer enhanced charge transfer between different ions and modified electronic structures to lower the kinetic energy barriers of the electrochemical processes.[8,10]

Designing proper structures for the battery-type electrode materials may greatly promote their electrochemical performance.[10,11] Hollow structures with high surface area, rich active sites, shortened distance for charge transfer and reduced aggregation of nanoscale subunits have been widely used in many energy related applications.[12–16] Among various hollow architectures, complex multi-shelled hollow structures have been demonstrated to exhibit better performance than conventional simple hollow structures.[17–19] Specifically, improved energy densities can be obtained from multi-shelled electrode materials as a result of higher content of active species within the hollow particles. Moreover, interconnection of neighboring shells can also enhance the structural robustness for better cycling stability.[20] As a result, fabrication of electrode materials with multi-shelled structures might be one effective way to enhance the electrochemical performance of HSCs.

Metal-organic frameworks (MOFs) constructed from a wide range of metal ions and organic linkers have been considered as appealing precursors to synthesize functional materials with complex structures and tailored compositions for energy related applications.[21–29] Although a large family of MOFs has been reported, conventional MOF-derived synthesis is mainly based on some simple MOF crystals. Complex designed MOF precursors are only limited to very few MOFs and composite MOF precursors with hollow, core-shell or hierarchical structures.[30–32] Therefore, delicate design and preparation of MOF precursors with novel structures and tailored compositions may significantly expand the toolbox for the construction of desirable structured functional materials.

Herein, a novel approach, combining chemical etching and sulfurization processes, is developed for synthesis of double-shelled zinc cobalt sulfide (Zn-Co-S) rhombic dodecahedral cages (RDCs) from bimetallic zinc/cobalt-based zeolitic imidazolate framework (Zn/Co-ZIF) rhombic dodecahedrons (RDs). Initially, Zn/Co-ZIF RDCs with a complex yolk-shelled structure are obtained through a chemical etching process. Selective partial etching of the Zn/Co-ZIF RDs results in the formation of yolk-shelled Zn/Co-ZIF RDCs without phase transition. Subsequently, the yolk-shelled Zn/Co-ZIF RDCs are further transformed into double-shelled Zn-Co-S RDCs via a solvothermal sulfurization reaction. When evaluated as a battery-type electrode material for HSCs, the obtained double-shelled Zn-Co-S RDCs exhibit higher specific capacitance and enhanced cycling stability compared with single-shelled Zn-Co-S RDCs.

The synthetic procedure of double-shelled Zn-Co-S RDCs is illustrated in **Figure 1**. First, bimetallic Zn/Co-ZIF RDs are synthesized by a previously reported method with a few modifications (see the Supporting Information for the experimental details).[33] The X-ray diffraction (XRD) pattern of the Zn/Co-ZIF sample shows typical diffraction peaks for (002), (112), (222), and (044) planes, which confirms the successful formation of ZIFs (Supporting Information, Figure S1a).[34] Field-

emission scanning electron microscopy (FESEM) image exhibits that the obtained Zn/Co-ZIF particles are uniform with a size of about 1.9 μm (Supporting Information, Figure S2a). These bimetallic MOF crystals show a typical rhombic dodecahedral morphology with smooth surfaces (**Figure 2**a). Transmission electron microscopy (TEM) image demonstrates the solid nature of Zn/Co-ZIF RDs (Figure 2b).

The as-prepared Zn/Co-ZIF RDs are converted into yolk-shelled Zn/Co-ZIF RDCs via a chemical etching process (step (i) in Figure 1). Tannic acid is used as the etching agent. The etching preferentially occurs under the surface layer of the Zn/Co-ZIF RDs, generating unique yolk-shelled RDCs.[35] As revealed by the XRD analysis, the crystal structure of the as-prepared yolk-shelled particles remains the same as that of Zn/Co-ZIF RDs, indicating that no phase transformation or new product generation occurs during the chemical etching process (Supporting Information, Figure S1b). The relatively low peak intensity in the XRD pattern of yolk-shelled Zn/Co-ZIF RDCs should be due to the partial etching and decomposition of the matrix of their Zn/Co-ZIF precursors. FESEM observation shows that the rhombic dodecahedral morphology is preserved after the chemical etching. The particle size of the yolk-shelled Zn/Co-ZIF RDCs is about 1.8 μm, which is slightly reduced compared with their Zn/Co-ZIF RD precursors (Supporting Information, Figure S2b). The surface of Zn/Co-ZIF RDCs becomes wrinkly after the chemical etching process (Figure 2c). The reduced particle size and changed surface topology are considered as the results of the etching-induced shrink of Zn/Co-ZIF RDs during the formation of yolk-shelled Zn/Co-ZIF RDCs. As elucidated by TEM observation, void space can be observed between the interior solid cores and the outer shells (Figure 2d and Supporting Information, Figure S3a-c). Moreover, the yolk-shelled structure is further confirmed by comparing the FESEM images of a broken Zn/Co-ZIF RD and cracked yolk-shelled Zn/Co-ZIF RDCs (Supporting Information, Figure S3d-f). The etching reaction induced by tannic acid is a surface functionalization-assisted

etching process.[35] Specifically, the surface layer of Zn/Co-ZIF RDs is absorbed and protected by tannic acid, as indicated by Fourier transform infrared analysis (Supporting Information, Figure S4).[36] However, tannic acid can hardly diffuse into the MOF particles owing to the large molecular size. Therefore, the partial etching of the unprotected inner cores leads to the formation of the yolk-shelled Zn/Co-ZIF RDCs.

The sulfurization process is conducted by a solvothermal treatment of the yolk-shelled Zn/Co-ZIF RDCs at 150 ^{o}C using thioacetamide as the sulfidation agent (step (ii) in Figure 1). XRD analysis shows the amorphous nature of the as-derived sample after the sulfurization treatment (Supporting Information, Figure S5). Energy-dispersive X-ray (EDX) spectrum reveals that the obtained Zn-Co-S particles possess a Zn/Co molar ratio of 0.6:1 (Supporting Information, Figure S6). As shown in the FESEM image at low magnification, uniform Zn-Co-S RDCs with a size of about 1.6 μm are obtained (Supporting Information, Figure S2c). The Zn-Co-S RDCs preserve the rhombic dodecahedral morphology with rough surfaces (**Figure 3**a). From a broken Zn-Co-S RDC shown in Figure 3b, a shell-in-shell hollow structure can be clearly observed. The structure of as-derived double-shelled Zn-Co-S RDCs is further elucidated by TEM characterization. As shown in Figure 3c, well-defined double-shelled structures can be clearly discerned. Moreover, a magnified TEM image of a single particle unambiguously indicates that both the inner and outer shells of the Zn-Co-S RDC possess rhombic dodecahedral structures (Figure 3d). A closer observation on the shells of a Zn-Co-S RDC reveals that the two shells with a similar thickness of about 120 nm are constructed by nanoparticles with a size of about 55 nm (Figure 3e and Supporting Information, Figure S7). As revealed by high-angle annular dark-field scanning transmission electron microscopy (HAADF-STEM) and elemental mapping images, Zn, Co, and S elements are evenly distributed in the shells of the Zn-Co-S RDC (Figure 3f). Therefore, through the sequential chemical etching and sulfurization method, nanoparticle-

constructed double-shelled Zn-Co-S RDCs are obtained, which are expected to exhibit high surface area, abundant active sites, facilitated mass/charge transport and reduced aggregation of subunits for enhanced electrochemical performance.

The sequential chemical etching and sulfurization strategy can be further applied to prepare double-shelled Zn-Co-S RDCs with different Zn/Co molar ratios. By simply adjusting the ratio of zinc/cobalt nitrate precursors during the synthesis of Zn/Co-ZIF RDs, double-shelled Zn-Co-S RDCs with Zn/Co molar ratios of 0.9:1 and 2:1 are obtained as determined by EDX spectra (Supporting Information, Figures S8 and S9). The morphological and structural evolution from the corresponding Zn/Co-ZIF RD precursors to their derived double-shelled Zn-Co-S RDCs are shown in Figure S10 and Figure S11 (Supporting Information).

For better comparison, single-shelled Zn-Co-S RDCs are also synthesized by direct sulfurization of bimetallic Zn/Co-ZIF RDs. The obtained uniform single-shelled Zn-Co-S RDCs show the well-defined rhombic dodecahedral structure with a particle size of about 1.9 μm (Supporting Information, Figure S12a,b). The magnified FESEM and TEM images of the sample clearly demonstrate a single-shelled hollow structure (Supporting Information, Figure S12c,d). The single-shelled Zn-Co-S RDCs are also amorphous as indicated by the XRD pattern (Supporting Information, Figure S13) and exhibit similar elemental composition compared with the double-shelled Zn-Co-S RDCs as shown by EDX spectrum (Supporting Information, Figure S14).

The electrode performance of the double-shelled and single-shelled Zn-Co-S RDCs is evaluated by using a three-electrode cell in 6.0 M KOH solution. A pair of redox peaks can be observed from each of the cyclic voltammetry (CV) curves of both double-shelled and single-shelled Zn-Co-S RDCs in a voltage window of 0 to 0.55 V versus a standard calomel electrode (SCE) at sweep rates ranging from 1 to 20 mV s^{-1} (Supporting Information, Figure S15a and Figure S16a). The distinct peaks indicate the

existence of Faradaic redox reactions of Zn-Co-S during the electrochemical process. Furthermore, **Figure 4**a shows a representative CV curve of the double-shelled Zn-Co-S RDCs at the sweep rate of 1 mV s^{-1} along with CV curve of the single-shelled Zn-Co-S RDCs for comparison. Notably, a larger area is enclosed by the CV curve of the double-shelled Zn-Co-S RDCs, revealing more charges can be stored compared with the single-shelled Zn-Co-S RDCs. The galvanostatic charge-discharge curves of both double-shelled and single-shelled Zn-Co-S RDCs are collected at various current densities ranging from 1 to 20 A g^{-1} (Supporting Information, Figure S15b and Figure S16b). The nonlinear nature of the curves further confirms the Faradaic behavior of the Zn-Co-S samples. Moreover, the symmetric configurations of the galvanostatic charge-discharge curves at different current densities suggest the outstanding reversibility of the Faradaic redox reactions. The specific capacitance of the double-shelled and single-shelled Zn-Co-S RDCs can be calculated according to the discharge curves (Figure 4b). The double-shelled Zn-Co-S RDCs show specific capacitance of 1266, 1052, 890, 808, and 720 F g^{-1} at current densities of 1, 2, 5, 10, and 20 A g^{-1}, respectively. About 57% of the capacitance can be retained with a 20-fold increase in current density, indicating good rate performance of the double-shelled Zn-Co-S RDCs. On the other hand, the single-shelled Zn-Co-S RDCs exhibit similar rate performance but much lower capacitance. Compared with the single-shelled Zn-Co-S RDCs, the double-shelled Zn-Co-S RDCs are inferred to exhibit a higher weight fraction of active species and improved electric contact, which might contribute to the enhanced specific capacitance.[8,18,37-39] Moreover, the double-shelled Zn-Co-S RDCs prepared with higher Zn/Co molar ratios of 0.9:1 and 2:1 show lower specific capacitance in comparison with those with Zn/Co molar ratio of 0.6:1, suggesting that the composition of the ternary TMSs is also an important factor affecting the electrochemical properties (Supporting Information, Figure S17 and Figure S18). Repeated charge-discharge cycling at a current density of 10 A g^{-1} is conducted to investigate the cycling stability of both double-shelled and

single-shelled Zn-Co-S RDCs. Impressively, after 10,000 cycles 91% of the initial specific capacitance of the double-shelled Zn-Co-S RDCs is retained whereas the single-shelled Zn-Co-S RDCs show a capacitance loss of 19% (Figure 4c). As indicated by the FESEM and TEM images of electrode materials after cycling test, the structure of double-shelled Zn-Co-S RDCs is reasonably preserved, whereas severe deformation of single-shelled Zn-Co-S RDCs is observed after the charge/discharge processes (Supporting Information, Figure S19). Thus, it can be inferred that the enhanced cycling stability of double-shelled Zn-Co-S RDCs results in part from the improved structural robustness owing to the mutual support of the two neighboring shells.[20] The electrochemical performance of double-shelled Zn-Co-S RDCs compares favorably to those of many reported zinc/cobalt-sulfide based electrode materials for HSCs (Supporting Information, Table S1).

In summary, zinc-cobalt sulfide rhombic dodecahedral cages with a well-defined double-shelled hollow structure have been synthesized by a sequential chemical etching and sulfurization strategy. Starting from solid Zn/Co-ZIF rhombic dodecahedron precursors, complex yolk-shelled Zn/Co-ZIF rhombic dodecahedral cages are obtained by simple chemical etching in the first step, which are further transformed into double-shelled zinc-cobalt sulfide cages. When used as battery-type electrode materials for hybrid supercapacitors, these double-shelled zinc-cobalt sulfide cages exhibit enhanced specific capacitance and improved cycling stability compared with single-shelled cages. The developed synthetic method may inspire further capability on constructing complex hollow-structured materials for a variety of energy related applications.

Acknowledgements

X. W. L. acknowledges the funding support from the National Research Foundation (NRF) of Singapore via the NRF investigatorship (NRF-NRFI2016-04).

References

[1] P. Simon, Y. Gogotsi, B. Dunn, *Science* **2014**, *343*, 1210–1211.

[2] B. Dunn, H. Kamath, J.-M. Tarascon, *Science* **2011**, *334*, 928–935.

[3] G. Yu, X. Xie, L. Pan, Z. Bao, Y. Cui, *Nano Energy* **2013**, *2*, 213–234.

[4] S. Choudhury, R. Mangal, A. Agrawal, L. A. Archer, *Nat. Commun.* **2015**, *6*, 10101.

[5] P. Simon, Y. Gogotsi, *Nat. Mater.* **2008**, *7*, 845–854.

[6] L. Shen, L. Yu, H. B. Wu, X.-Y. Yu, X. Zhang, X. W. Lou, *Nat. Commun.* **2015**, *6*, 6694.

[7] L. Yu, B. Guan, W. Xiao, X. W. Lou, *Adv. Energy Mater.* **2015**, *5*, 1500981.

[8] B. Y. Guan, L. Yu, X. Wang, S. Song, X. W. Lou, *Adv. Mater.* **2017**, *29*, 1605051.

[9] X.-Y. Yu, L. Yu, X. W. Lou, *Adv. Energy Mater.* **2016**, *6*, 1501333.

[10] Y. M. Chen, Z. Li, X. W. Lou, *Angew. Chem. Int. Ed.* **2015**, *54*, 10521–10524.

[11] L. Shen, L. Yu, X.-Y. Yu, X. Zhang, X. W. Lou, *Angew. Chem. Int. Ed.* **2015**, *54*, 1868–1872.

[12] X. W. Lou, L. A. Archer, Z. Yang, *Adv. Mater.* **2008**, *20*, 3987–4019.

[13] L. Yu, H. B. Wu, X. W. Lou, *Acc. Chem. Res.* **2017**, *50*, 293–301.

[14] L. Yu, H. Hu, H. B. Wu, X. W. Lou, *Adv. Mater.* **2017**, DOI: 10.1002/adma.201604563.

[15] B. Y. Guan, L. Yu, J. Li, X. W. Lou, *Sci. Adv.* **2016**, *2*, e1501554.

[16] B. Y. Guan, L. Yu, X. W. Lou, *Adv. Mater.* **2016**, *28*, 9596–9601.

[17] X.-Y. Yu, L. Yu, L. Shen, X. Song, H. Chen, X. W. Lou, *Adv. Funct. Mater.* **2014**, *24*, 7440–7446.

[18] H. Hu, B. Guan, B. Xia, X. W. Lou, *J. Am. Chem. Soc.* **2015**, *137*, 5590–5595.

[19] B. Y. Guan, L. Yu, X. W. Lou, *Angew. Chem. Int. Ed.* **2017**, *56*, 2386–2389.

[20] H. Hu, B. Y. Guan, X. W. Lou, *Chem* **2016**, *1*, 102–113.

[21] W. Xia, A. Mahmood, R. Zou, Q. Xu, *Energy Environ. Sci.* **2015**, *8*, 1837–1866.

[22] T. Y. Ma, S. Dai, M. Jaroniec, S. Z. Qiao, *J. Am. Chem. Soc.* **2014**, *136*, 13925–13931.

[23] Z. Zhang, Y. Chen, S. He, J. Zhang, X. Xu, Y. Yang, F. Nosheen, F. Saleem, W. He, X. Wang, *Angew. Chem. Int. Ed.* **2014**, *53*, 12517–12521.

[24] X.-Y. Yu, L. Yu, H. B. Wu, X. W. Lou, *Angew. Chem. Int. Ed.* **2015**, *54*, 5331–5335.

[25] H. Hu, L. Han, M. Yu, Z. Wang, X. W. Lou, *Energy Environ. Sci.* **2016**, *9*, 107–111.

[26] L. Zhang, H. B. Wu, X. W. Lou, *J. Am. Chem. Soc.* **2013**, *135*, 10664–10672.

[27] L. Zhang, H. B. Wu, S. Madhavi, H. H. Hng, X. W. Lou, *J. Am. Chem. Soc.* **2012**, *134*, 17388–17391.

[28] G. Lu, S. Li, Z. Guo, O. K. Farha, B. G. Hauser, X. Qi, Y. Wang, X. Wang, S. Han, X. Liu, et al., *Nat. Chem.* **2012**, *4*, 310–316.

[29] H. Hu, J. Zhang, B. Guan, X. W. Lou, *Angew. Chem. Int. Ed.* **2016**, *55*, 9514–9518.

[30] L. Han, X.-Y. Yu, X. W. Lou, *Adv. Mater.* **2016**, *28*, 4601–4605.

[31] J. Yang, F. Zhang, H. Lu, X. Hong, H. Jiang, Y. Wu, Y. Li, *Angew. Chem. Int. Ed.* **2015**, *54*, 10889–10893.

[32] B. Y. Guan, L. Yu, X. W. Lou, *Energy Environ. Sci.* **2016**, *9*, 3092–3096.

[33] J. Cravillon, R. Nayuk, S. Springer, A. Feldhoff, K. Huber, M. Wiebcke, *Chem. Mater.* **2011**, *23*, 2130–2141.

[34] K. S. Park, Z. Ni, A. P. Côté, J. Y. Choi, R. Huang, F. J. Uribe-Romo, H. K. Chae, M. O'Keeffe, O. M. Yaghi, *Proc. Natl. Acad. Sci.* **2006**, *103*, 10186–10191.

[35] M. Hu, Y. Ju, K. Liang, T. Suma, J. Cui, F. Caruso, *Adv. Funct. Mater.* **2016**, *26*, 5827–5834.

[36] M. Arshad, A. BegS, Z. A. Siddiqui, *Macromol. Mater. Eng.* **1969**, *7*, 67–78.

[37] Y. J. Hong, M. Y. Son, Y. C. Kang, *Adv. Mater.* **2013**, *25*, 2279–2283.

[38] J. Wang, H. Tang, H. Ren, R. Yu, J. Qi, D. Mao, H. Zhao, D. Wang, *Adv. Sci.* **2014**, *1*, 1400011.

[39] X. Wang, X.-L. Wu, Y.-G. Guo, Y. Zhong, X. Cao, Y. Ma, J. Yao, *Adv. Funct. Mater.* **2010**, *20*, 1680–1686.

Figures and Captions

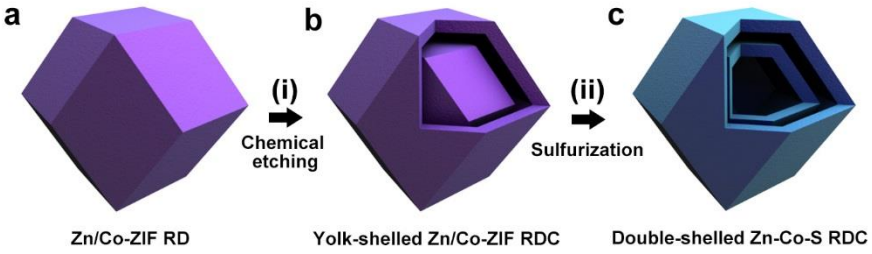

Figure 1. Schematic illustration of the formation process of double-shelled Zn-Co-S RDCs. Step (i): transformation of (a) Zn/Co-ZIF RD into (b) yolk-shelled Zn/Co-ZIF RDC by chemical etching. Step (ii): conversion of yolk-shelled Zn/Co-ZIF RDC into (c) double-shelled Zn-Co-S RDC via a sulfurization treatment.

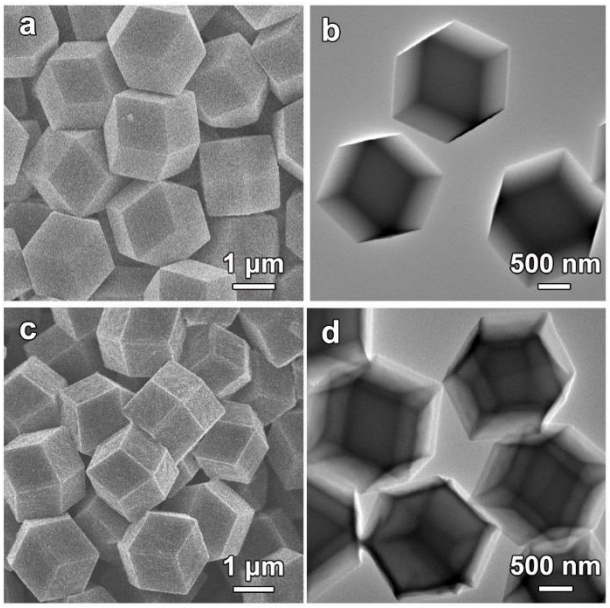

Figure 2. (a,c) FESEM images and (b,d) TEM images of (a,b) Zn/Co-ZIF RDs and (c,d) yolk-shelled Zn/Co-ZIF RDCs.

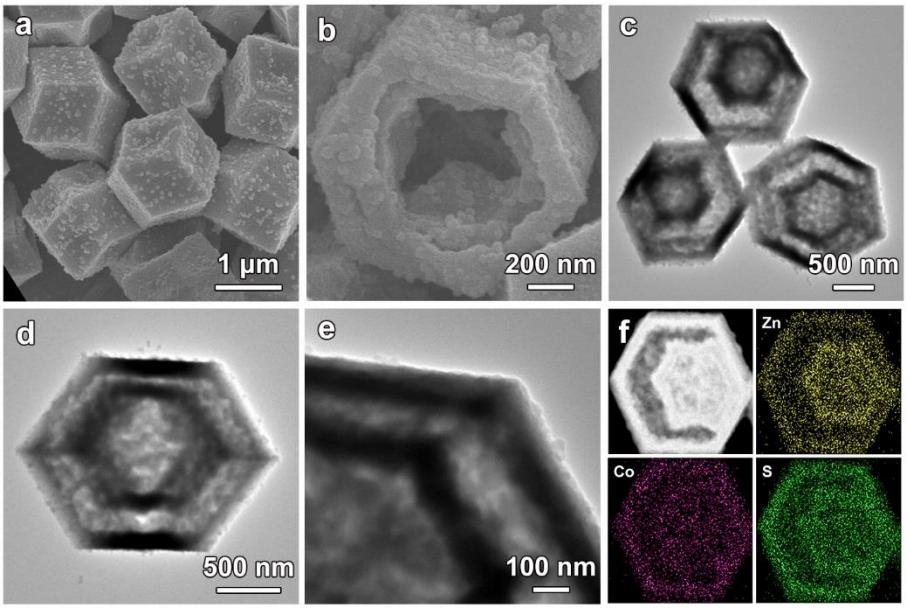

Figure 3. (a,b) FESEM images and (c-e) TEM images of double-shelled Zn-Co-S RDCs. (f) HAADF-STEM image and elemental mappings for Zn, Co, and S of a double-shelled Zn-Co-S RDC.

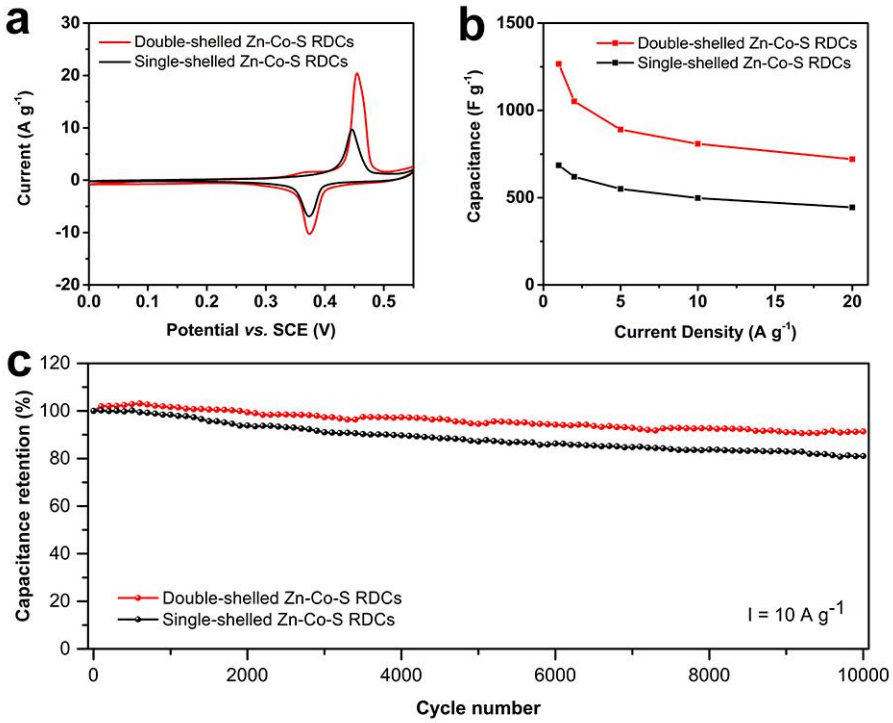

Figure 4. (a) CV curves of double-shelled and single-shelled Zn-Co-S RDCs at a sweep rate of 1 mV s^{-1}. (b) Specific capacitance at different current densities. (c) Cycling performance at a constant current density of 10 A g^{-1}.

for Table of Content Entry

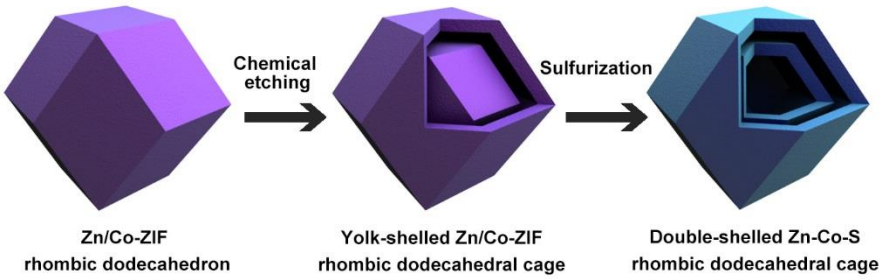

Double-shelled zinc-cobalt sulfide rhombic dodecahedral cages are synthesized by a sequential chemical etching and sulfurization strategy. With the structural advantages, the well-defined double-shelled zinc-cobalt sulfide cages exhibit much enhanced electrochemical performance compared to the single-shelled counterpart as electrode materials for hybrid supercapacitors.